

A Novel Square-Root Adaptive Unscented Kalman Filtering Method for Accurate State-of-Charge Estimation of Lithium-ion Batteries

Shunli Wang^{1,*}, Haiying Gao¹, Jialu Qiao¹, Jie Cao¹, Carlos Fernandez²

¹ School of information engineering, Southwest University of science and technology, Mianyang, Sichuan 621010, China;

² School of Pharmacy and Life Science, Robert Gordon University, Aberdeen AB10-7GJ, UK

*E-mail: 497420789@qq.com

Received: 2 March 2022 / Accepted: 28 April 2022 / Published: 6 June 2022

The accurate state-of-charge estimation of the lithium-ion battery is one of the key technologies to benchmark the rapid development of new energy vehicles. Unscented Kalman filtering abandons the traditional way of forcing the system to linearize, selects the symmetric sampling strategy to obtain sampling points, and uses Unscented Transformation to deal with the nonlinear transfer of mean and covariance. Then calculate the statistical properties of nonlinear functions with the corresponding weights of each sampling point. However, the traditional unscented Kalman filtering has accumulated errors due to a large number of calculations, the covariance matrix is easy to diverge due to the inability to perform QR decomposition, and the system has deviations caused by unknown noise, resulting in low stability and easy divergence of the state-of-charge estimation results. Based on the second-order RC equivalent circuit model, a square-root adaptive unscented Kalman filtering is proposed, which replaces the state error covariance matrix with the square root of the state error covariance matrix. The noise covariance is updated in real-time to improve the tracking and convergence of state-of-charge estimation results. The algorithm is verified by the Hybrid Pulse Power Characterization test (HPPC) and Beijing Bus Dynamic Stress Test (BBDST) working conditions. The results show that square-root adaptive unscented Kalman filtering can improve the estimation accuracy of state-of-charge under complex working conditions.

Keywords: Lithium-ion battery; Second-order RC equivalent circuit model; State of Charge; Square-Root Adaptive Unscented Kalman Filtering

1. INTRODUCTION

After human society entered the industrial civilization, the development model highly depends on fossil energy and material resource inputs, resulting in a large amount of carbon emissions, energy consumption, and environmental problems, leading to global climate change and unsustainable

development[1]. Facing the severe situation of tight resource constraints, serious environmental pollution, and ecosystem degradation, vigorously developing new energy has become an irreversible trend[2]. In the use of fossil fuels in China, automobile fuel consumption accounts for 70% of the total oil consumption, which shows that the market competition for new energy vehicles will become increasingly fierce in the future[3]. As one of the core components of the "three electricity" of new energy vehicles, the lithium-ion battery industry has also ushered in a new round of development opportunities[4]. Judging from the competition pattern of the power battery market today, the unique cathode material of ternary lithium-ion battery makes the battery have a high energy density, long service life, and low cost, which makes it occupy the mainstream position[5]. However, under the influence of capital and policies, the advanced productivity of our country's power battery industry is insufficient and high-quality resources are scarce, resulting in the overcapacity of lithium-ion batteries[6]. Accurate state of charge estimation is one of the keys to improving the efficiency of power battery usage.

At present, the common equivalent circuit models of lithium-ion batteries include Rint model, Thevenin model, PNGV model, GNL model, second-order RC model, etc[7]. Simple models are good for parameter identification, but cannot accurately describe the batteries working characteristics; higher-order models can represent battery characteristics in more detail, but the amount of computation will increase significantly and it's not practical[8]. Considering the precise modeling and model simplification, and comparing the influence of different orders on SOC estimation results, the accuracy of models above the second-order is increased inconspicuous, but the computational effort is significantly larger[9]. The ampere integral method estimates SOC by accumulating the charge and discharge. The discharge test method is to discharge the battery at a constant current to the cut-off voltage and multiply the current by the discharge time as the remaining capacity of the battery[10, 11]. According to the relationship between the open-circuit voltage and the lithium-ion concentration in the battery, the open-circuit voltage method indirectly fits the corresponding relationship between the open-circuit voltage and SOC[12]. The neural network method trains the system through a large number of comprehensive data and then inputs the sample data into the system to obtain the estimated SOC value[13, 14]. Kalman filtering method makes the optimal estimation of the state of the complex dynamic system according to the minimum mean square error[15]. Because of the complex internal structure of the lithium-ion battery, the charge and discharge are often accompanied by polarization effect, current accumulation effect, ohmic effect, etc[16]. The battery is aging after self-discharge and repeated recycling, and it shows strong nonlinearity under complex working conditions, so it is difficult for the traditional SOC estimation algorithm of lithium-ion battery to obtain a real-time and effective state of charge[17, 18]. Therefore, the innovation and improvement of the algorithm for lithium-ion battery SOC estimation is particularly important for its long-term development and commercial application[19].

Aiming at the potential problem of filter divergence caused by the failure of Cholesky decomposition of state error covariance matrix in the original UKF algorithm, and the deviation caused by unknown noise in the system, considering the accuracy of characterization and computational complexity, the second-order RC equivalent circuit model of lithium-ion battery is established in this paper. The Recursive least square (RLS) method is used for online parameter identification, and the square-root adaptive unscented Kalman filter is used to estimate the SOC of lithium-ion battery. The accuracy of the algorithm is verified by the estimation results of SOC under different working conditions.

2. THEORETICAL ANALYSIS

2.1. Modeling of second-order RC equivalent circuit

Reasonable selection of lithium-ion battery model is important for accurate estimation of SOC. Many models that are widely used at present. The Thevenin model[20] only considers the rapid change of the battery polarization response; the Rint model[21] does not consider the polarization characteristics of the battery, so the accuracy is not ideal; the PNGV model[22] has high accuracy in simulating transient response, and is suitable for high current step-type and complex charging discharge conditions, but not for this paper. Compared with other models, the second-order RC equivalent circuit model not only fully considers the slow change process of the battery polarization reaction, but also has a small amount of calculation and high accuracy, so it is chosen in this paper. The second-order RC equivalent circuit model for lithium-ion batteries is shown in Figure 1, where U_{OC} stands for open-circuit voltage; U_L denotes the terminal voltage; R_0 is Ohm internal resistance, and the voltage on R_0 is an ohm voltage, which represents the instantaneous voltage drop when the battery is charged or discharged. R_p and C_p denotes polarized resistance and capacitance. The RC loop consisting of R_{p1} and C_{p1} represents the electrochemical polarization process in which the voltage of the battery changes rapidly when the current changes; The RC circuit composed of R_{p2} and C_{p2} indicates the concentration process of slow and stable voltage during the internal chemical reaction of the battery. $I(t)$ indicates the current of the loop and specifies that the direction of discharge is positive.

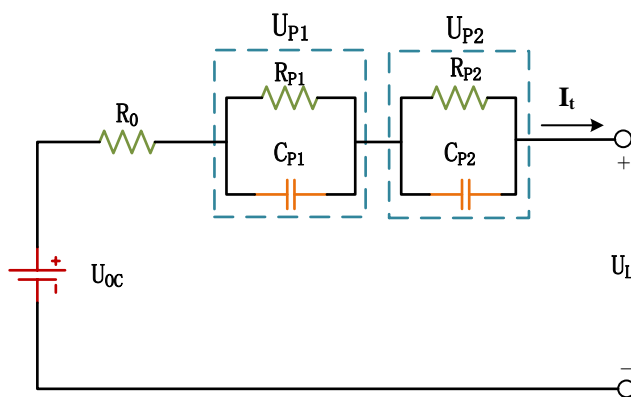


Figure 1. Second-Order RC equivalent circuit model

According to the second-order RC equivalent circuit model and Kirchhoff's law, the voltage and current expressions of the circuit can be listed as Equation (1). Set SOC_0 is the initial value of the state, and the battery SOC can be obtained by the ampere-hour integration method, as shown in Equation (2). Where the η Coulomb efficiency is usually taken as 1, and Q_N is the rated capacity of the battery.

$$\begin{cases} U_{L,t} = U_{OC} - I_t R_0 - U_{p1,t} - U_{p2,t} \\ I_t = \frac{U_{p1,t}}{R_{p1}} + C_{p1} \frac{dU_{p1,t}}{dt} = \frac{U_{p2,t}}{R_{p2}} + C_{p2} \frac{dU_{p2,t}}{dt} \end{cases} \quad (1)$$

$$SOC_t = SOC_0 - \frac{\eta}{Q_N} \int_0^t I_t dt \tag{2}$$

According to the equivalent circuit model and Equation (1), $x_k = [SOC_k U_{P1} U_{P2}]^T$ selected as the state variable, i_k as the system input variable, $y_k = [U_{L,k}]$ as the output variable, after discretizing the SOC definition, the state space equation after discretization can be listed as Equation (3), where Δt represents the sampling time interval.

$$\left\{ \begin{aligned} x_{k+1} &= \begin{bmatrix} 1 & 0 & 0 \\ 0 & e^{-\frac{\Delta t}{R_{P1}C_{P1}}} & 0 \\ 0 & 0 & e^{-\frac{\Delta t}{R_{P2}C_{P2}}} \end{bmatrix} x_k + \begin{bmatrix} -\Delta t/Q_N \\ R_{P1} \left(1 - e^{-\frac{\Delta t}{R_{P1}C_{P1}}}\right) \\ R_{P2} \left(1 - e^{-\frac{\Delta t}{R_{P2}C_{P2}}}\right) \end{bmatrix} i_k + w_k \\ y_k &= U_{oc,k} - R_0 i_k + \begin{bmatrix} 0 \\ -1 \\ -1 \end{bmatrix}^T x_k + v_k \end{aligned} \right. \tag{3}$$

In the Equation (3), w_k is the system noise at the k moment, and v_k is the measurement error at the k moment.

2.2. Recursive least square online parameter identification

Recursive least square (RLS) is a model parameter identification and data mining algorithm based on adaptive filtering theory, which is a learning process to solve the least square loss function recursively to obtain the optimal solution to the problem. It adopts the method of regularly correcting and updating system parameters, which can be applied to the situation that the system model and parameters are greatly affected by external conditions, and can accurately capture the real-time characteristics of the system.

The discrete equations of the model to be identified and the corresponding difference equations are shown in Equation (4).

$$\left\{ \begin{aligned} G(z) &= \frac{y(z)}{u(z)} = \frac{b_1 z^{-1} + b_2 z^{-2} + \dots + b_n z^{-n}}{1 + a_1 z^{-1} + a_2 z^{-2} + \dots + a_n z^{-n}} \\ y(k) &= - \sum_{i=1}^n a_i y(k-i) + \sum_{i=1}^n b_i u(k-i) + v(k) \end{aligned} \right. \tag{4}$$

Where a, b are the parameters to be estimated; $y(k)$ is the k-time observation value of the system output; $u(k)$ is the k-time value of the system input; and $v(k)$ is the random noise with the mean value of 0.

Convert the battery model into the least-squares mathematical form, as shown in the Equation (5).

$$U_{oc} = \left(\frac{R_{P1}}{R_{P1}C_{P1}s + 1} + \frac{R_{P2}}{R_{P2}C_{P2}s + 1} + R_0 \right) I + U_L \tag{5}$$

Let the time constant $\tau_1 = R_{P1}$, $C_{P1}\tau_2 = R_{P2}C_{P2}$, set $a = \tau_1\tau_2$, $b = \tau_1 + \tau_2$, $c = R_{P1} + R_{P2} + R_0$, $d = R_{P1}\tau_2 + R_{P2}\tau_1 + R_0(\tau_1 + \tau_2)$, then the equation can be rewritten as shown in the Equation (6).

$$aU_{OC}s^2 + bU_{OC}s + U_{OC} = aR_0Is^2 + dIs + cI + aU_Ls^2 + bU_Ls + U_L \tag{6}$$

Substitute $s = [x(k) - x(k - 1)]/Ts^2 = [x(k) - 2x(k - 1) + x(k - 2)]/T^2$ into Equation (6) and discretize it as shown in Equation (7), where T is the sampling time, set to 0.1 s.

$$U_{OC}(k) - U_L(k) = \frac{-bT - 2a}{T^2 + bT + a}[U_L(k - 1) - U_{OC}(k - 1)] + \frac{a}{T^2 + bT + a}[U_L(k - 2) - U_{OC}(k - 2)] + \frac{cT^2 + dT + aR_0}{T^2 + bT + a}I(k) + \frac{-dT - 2aR_0}{T^2 + bT + a}I(k - 1) + \frac{aR_0}{T^2 + bT + a}I(k - 2) \tag{7}$$

For the convenience of identification, the fractional expression in the above equation is replaced by the actual parameters $k_1 \sim k_5$, and the optimized expression result is shown in Equation (8).

$$U_{OC}(k) - U_L(k) = k_1[U_L(k - 1) - U_{OC}(k - 1)] + k_2[U_L(k - 2) - U_{OC}(k - 2)] + k_3I(k) + k_4I(k - 1) + k_5I(k - 2)$$

Substitute Equation (8) into recursive least-squares and substitute $\theta = [k_1 \ k_2 \ k_3 \ k_4 \ k_5]^T$ into the algorithm as the parameter vector to be identified. Then the circuit model parameter $R_0 \ \& \ R_{P1} \ \& \ R_{P2} \ \& \ C_{P1} \ \& \ C_{P2}$ can be deduced, and the result is as shown in Equation (9).

$$\left\{ \begin{array}{l} R_0 = \frac{k_5}{k_2} \\ R_{P1} = \frac{(\tau_1 c + \tau_2 R_0 - d)}{(\tau_1 - \tau_2)} \\ R_{P2} = c - R_{P1} - R_0 \\ C_{P1} = \frac{\tau_1}{R_{P1}} \\ C_{P2} = \frac{\tau_2}{R_{P2}} \end{array} \right. \tag{9}$$

2.3. Square root adaptive traceless Kalman algorithm

Compared with KF and EKF, UKF does not ignore higher-order terms when dealing with nonlinear problems but uses data reconstruction to infinitely approximate the true value, so it has higher estimation accuracy and stronger robustness. However, the UKF itself still has deficiencies. In this paper, the SR-AUKF is proposed to focus on solving the following two problems.

(1) Due to system noise and calculation errors, the traditional UKF algorithm may cause the error covariance matrix to be negatively determined, resulting in divergent prediction results. The SR-AUKF algorithm uses the square root of the covariance instead of the covariance to participate in the iterative operation, which ensures the numerical stability of the filtering algorithm and improves the accuracy and reliability of the filtering result tracking.

(2) KF and its derivative algorithms EKF, UKF, etc. are substituted for process noise and observation noise at fixed values, but in fact, the noise of the system is time-varying. In this paper, the Sage-Husa adaptive algorithm is combined with SR-UKF to propose an SR-AUKF based on online parameter recognition.

The calculation process of the SR-AUKF algorithm is shown in Equation (10 – 21).

(1) Data initialization

$$\begin{cases} \hat{x}_0 = E[x_0] \\ S_0 = chol\{E[(x_0 - \hat{x}_0)(x_0 - \hat{x}_0)^T]\} \\ \sqrt{Q_0} = S_0 \\ \sqrt{R_0} = chol\{E[(y_0 - \hat{y}_0)(y_0 - \hat{y}_0)^T]\} \end{cases} \quad (10)$$

(2) Forecast phase

Compute the matrix constructed from sigma points:

$$\chi_{k-1} = [\hat{x}_{k-1} \quad \hat{x}_{k-1} + \sqrt{L + \lambda} S_k \quad \hat{x}_{k-1} - \sqrt{L + \lambda} S_k] \quad (11)$$

After sampling the Sigma points, the set of sigma points is nonlinearly transformed by the state equation, and the square root of the state and variance is further predicted:

$$\begin{cases} \chi_{i,k-1}^* = A_{k-1} \chi_{i,k-1} + B_{k-1} u_{k-1} \\ \hat{x}_{k|k-1}^i = \sum_{i=0}^{2L} \omega_i^m \chi_{i,k|k-1}^* \\ S_{k|k-1}^* = qr \left\{ \left[\sqrt{\omega_i^c} [\chi_{1:2n,k|k-1}^* - \hat{x}_{k|k-1}] \sqrt{Q_{k-1}} \right] \right\} \\ S_{k|k-1} = cholupdate \left\{ S_{k|k-1}^*, [\chi_{0,k|k-1}^* - \hat{x}_{k|k-1}], \sqrt{\omega_0^c} \right\} \end{cases} \quad (12)$$

(3) Update Phase

Sigma point resampling:

$$\chi_{k|k-1} = [\hat{x}_{k|k-1} \quad \hat{x}_{k|k-1} + \sqrt{L + \lambda} S_{k|k-1} \quad \hat{x}_{k|k-1} - \sqrt{L + \lambda} S_{k|k-1}] \quad (13)$$

The sigma point is nonlinearly transformed by the measurement equation and the residuals are calculated:

$$\begin{cases} \hat{y}_{k|k-1} = C_k \chi_{k|k-1} + D_k u_k \\ \hat{y}_k = \sum_{i=0}^{2L} \omega_i^m \hat{y}_{i,k|k-1} \\ e_k = y_k - \hat{y}_k \end{cases} \quad (14)$$

Estimate update measurement noise statistical characteristics:

$$\begin{cases} \sqrt{R^{**}} = cholupdate \left\{ \sqrt{1 - d_k} \sqrt{\hat{R}_{k-1}}, |e_k|, d_k \right\} \\ \sqrt{R^*} = cholupdate \left\{ \sqrt{R^{**}}, \hat{y}_{0:2L,k|k-1} - \hat{y}_k, -d_k \omega_i^c \right\} \\ \sqrt{\hat{R}_k} = diag \left\{ \sqrt{diag(\sqrt{R^*} \sqrt{R^{*T}})} \right\} \end{cases} \quad (15)$$

Calculate the variance matrix of the output variable at k moment:

$$\begin{cases} S_y^* = qr \left\{ \sqrt{\omega_i^c} (\hat{y}_{1:2n,k|k-1} - \hat{y}_{k|k-1}) \sqrt{R_k} \right\} \\ S_y = cholupdate \left\{ S_y^*, (\hat{y}_{0,k|k-1} - \hat{y}_k), \sqrt{\omega_0^c} \right\} \end{cases} \quad (16)$$

Calculate the covariance between the k moment state variable and the observed variable:

$$P_{xy} = \sum_{i=0}^{2L} \omega_i^c (\chi_{i,k|k-1}^* - \hat{x}_{k|k-1}) (y_{i,k|k-1} - \hat{y}_{k|k-1})^T \quad (17)$$

Calculate the Kalman filter gain:

$$K_k = \frac{P_{xy}/S_{y,k}^T}{S_{y,k}} \tag{18}$$

Update the corrected state variable:

$$\hat{x}_k = \hat{x}_{k|k-1} + K_k e_k \tag{19}$$

Solve for the square root of the posterior state variance:

$$\begin{cases} U = K_k S_{y,k} \\ S_k = cholupdate\{S_{k|k-1}, U, -1\} \end{cases} \tag{20}$$

Update the statistical characteristics of the estimated process noise:

$$\begin{cases} \sqrt{Q^{**}} = cholupdate\left\{\sqrt{\hat{Q}_{k-1}}, |\hat{x}_k - \hat{x}_{k|k-1}|, d_k\right\} \\ \sqrt{Q^*} = cholupdate\{\sqrt{Q^{**}}, U, -d_k\} \\ \sqrt{\hat{Q}_k} = diag\left\{\sqrt{diag\left(\sqrt{Q^*} \sqrt{Q^{*T}}\right)}\right\} \end{cases} \tag{21}$$

In this paper, RLS is used to identify the parameters of the second-order RC equivalent model online with the voltage and current data obtained from the experiment. Then the identified parameter results are substituted into the state space equation, and the battery SOC can be estimated through the above steps.

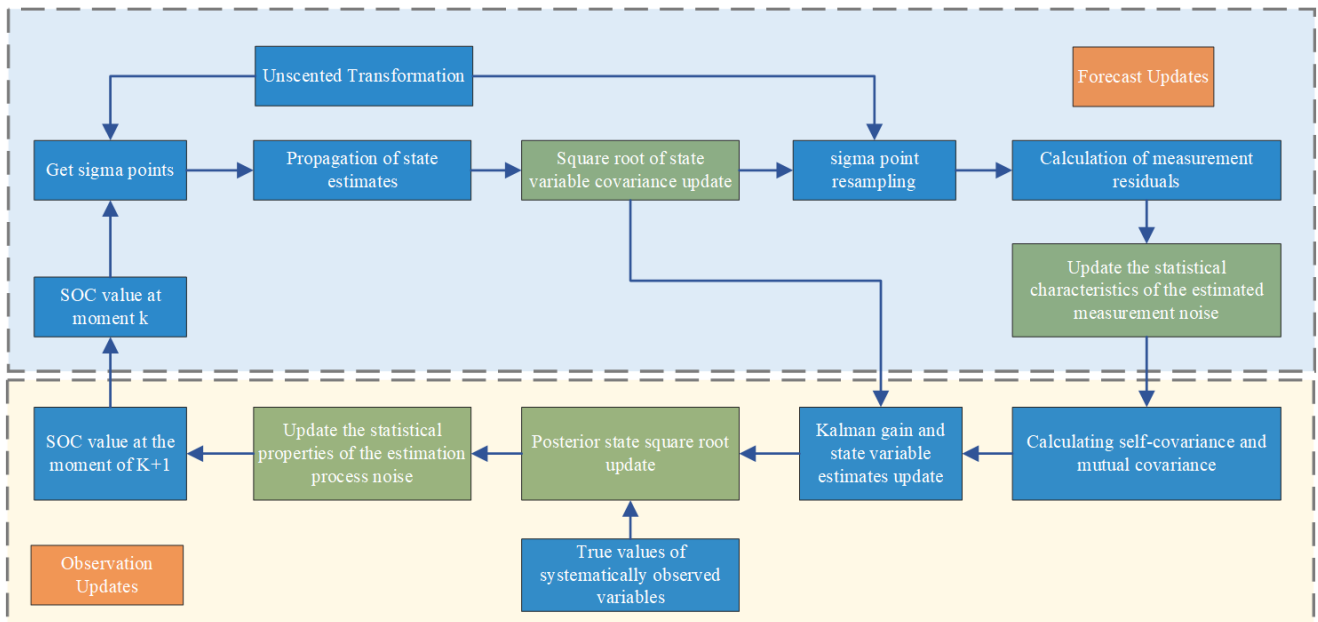


Figure 2. Schematic diagram of the implementation of the SR-AUKF algorithm

The algorithm implementation process of SR-AUKF is shown in Figure 2. The algorithm can solve two major problems of the traditional UKF, ensuring the matrix positive definite by transmitting the square root of the error covariance to make the algorithm stable, and improving the accuracy of SOC estimation by adding noise adaptation.

3. EXPERIMENTAL ANALYSIS

3.1. Test platform construction

To verify the accuracy of the battery model and algorithm, it is necessary to build an experimental platform to conduct experimental tests on the battery under different complex working conditions. The experimental object uses a lithium-ion aluminum shell battery with a nominal capacity of 45 Ah, and the entire battery test platform is shown in Figure 3. The BTS200-100-104 is used to test the battery, the TT-5166TH is used to provide a constant experimental temperature to the battery, and the host computer is used to record the experimental data in Figure 3.

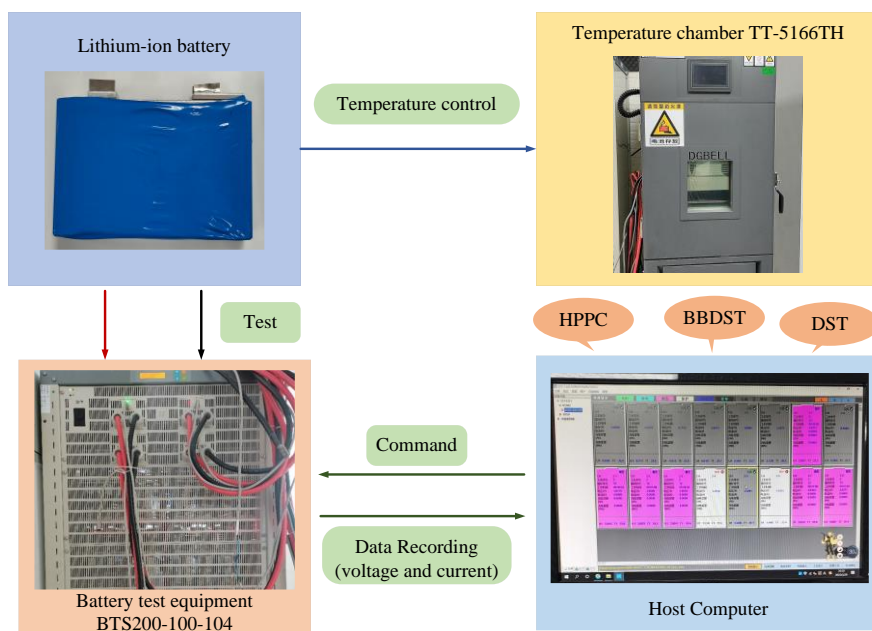


Figure 3. Battery test platform

3.2. Online parameter identification results

The battery parameter identification is carried out under the Hybrid Pulse Power Characterization (HPPC) working condition. The experimental object is a lithium-ion aluminum shell battery, the nominal capacity of the battery is 45 Ah, and the actual capacity is 43.4275 Ah. HPPC experiments are performed under a constant temperature of 27°C. The battery is discharged at a rate of 1 C, 10% SOC each time, starting from SOC=1 and ending at SOC=0, and parameter identification is carried out according to the current and voltage data obtained by the experiment. The steps of the HPPC experiment are as follows:

(1) Lithium-ion battery is fully charged with a constant voltage of 4.2 V and a constant current of 1 C.

(2) After charging, the battery was put on hold for 40 min, then discharged at a rate of 1 C for 10 s, and then put on hold for 40 s. Finally, charge the battery at a rate of 1 C for 10 s, and then put the battery on hold for 160 s, which is a complete pulse test.

(3) Discharge the battery at a rate of 1C for 6 minutes to reduce the battery capacity by 10%.

(4) Repeat steps (2) and (3) 10 times, and the battery open-circuit voltage U_{OC} is recorded after each charge until the battery capacity is zero.

Where SOC=0.7, the pulse test voltage curve is shown in Figure 4.

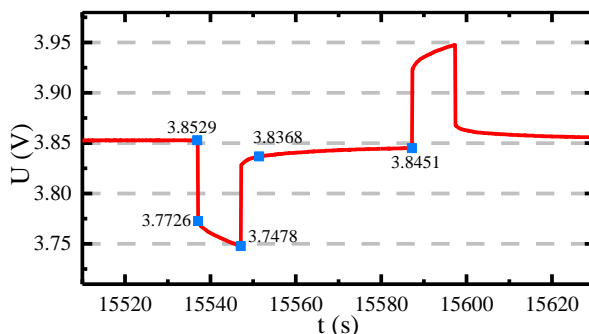
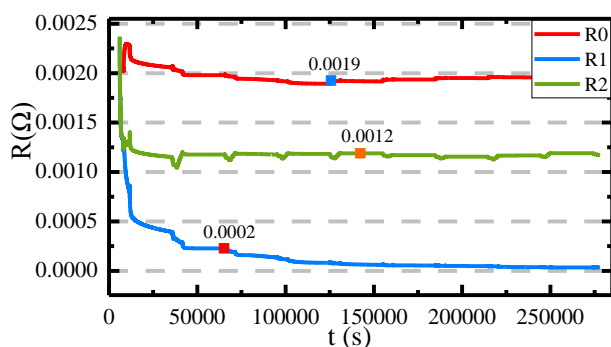
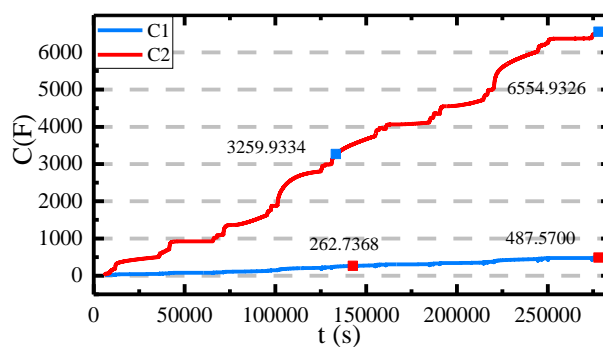


Figure 4. HPPC test voltage curve at SOC=0.7

The RLS algorithm is verified by the experimental data collected under HPPC working condition, and the dynamic changes of the internal parameters at different times are obtained. The results of dynamic parameter identification are shown in Figure 5.



(a) Resistance identification results under HPPC condition



(b) Capacitance identification results under HPPC condition

Figure 5. Parameter identification results under HPPC working condition

Based on the Thevenin model, H. W. He[23] used the off-line parameter identification method to obtain the maximum error of estimated voltage is 3.09%. And based on the second-order RC model, S. L. Liu[24] used the off-line parameter identification method to obtain the mean error of estimated voltage is 1.1%. However, in this paper, the maximum error of the online identification based on the second-order RC equivalent circuit can be controlled within 2% due to the severe chemical reactions inside the battery during charging and discharge, and the mean error is within 0.7%. The verification

results show that RLS algorithm has high online parameter identification accuracy and can obtain accurate model parameter values.

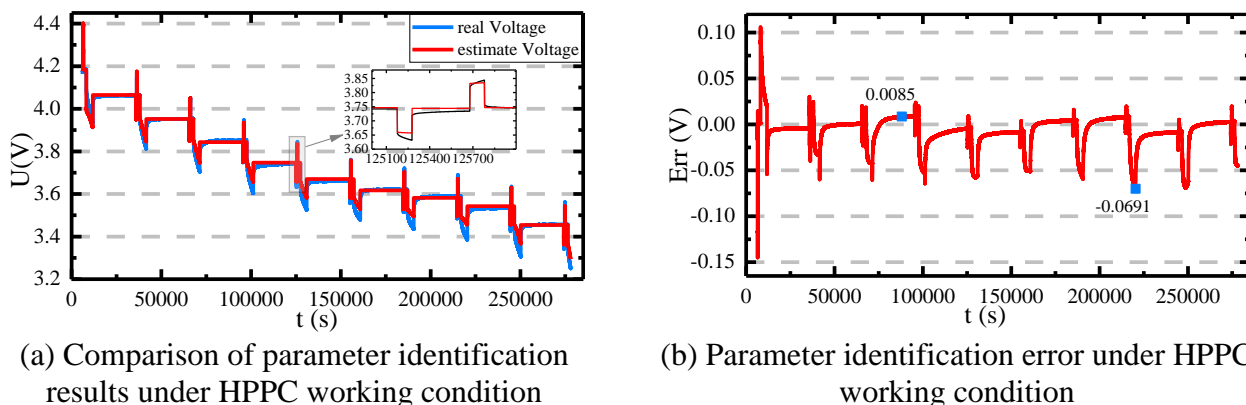


Figure 6. Parameter identification results under HPPC working condition

3.3. Experimental verification under DST working condition

To verify the accuracy of the online parameter identification results and the convergence of the SR-AUKF algorithm, the dynamic stress test (DST) working condition is used for verification. First, the battery was charged with 1 C constant current until the upper cut-off voltage of 4.2 V. After charging, the battery is shelved for 30 min to stabilize the battery voltage. Constant current discharge and constant current charge were performed at 0.5 C rate for 4 min, followed by constant current discharge at 1 C rate for 4 min. These three steps are cycled until the end of the discharge. The SOC values estimated by UKF and SR-AUKF are compared with the real values, and the obtained results and error diagrams are shown in Figure 7.

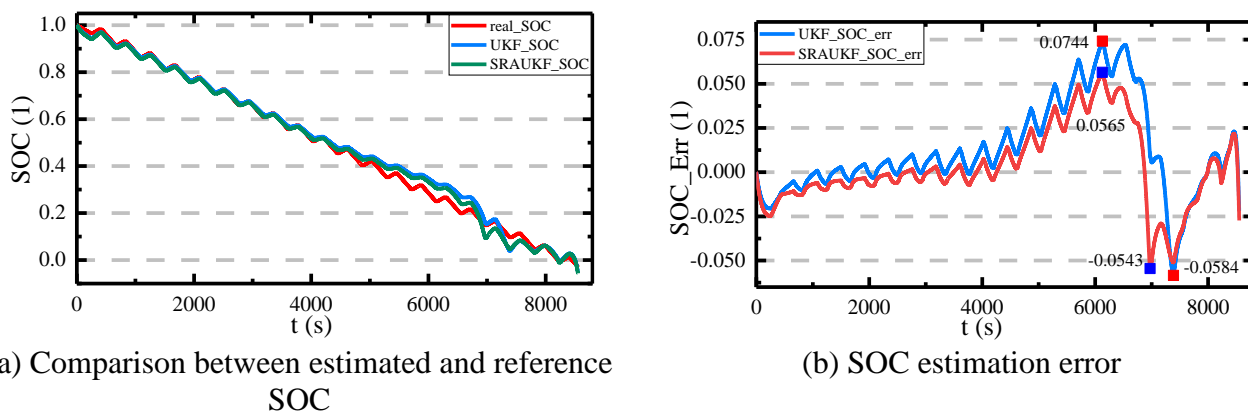


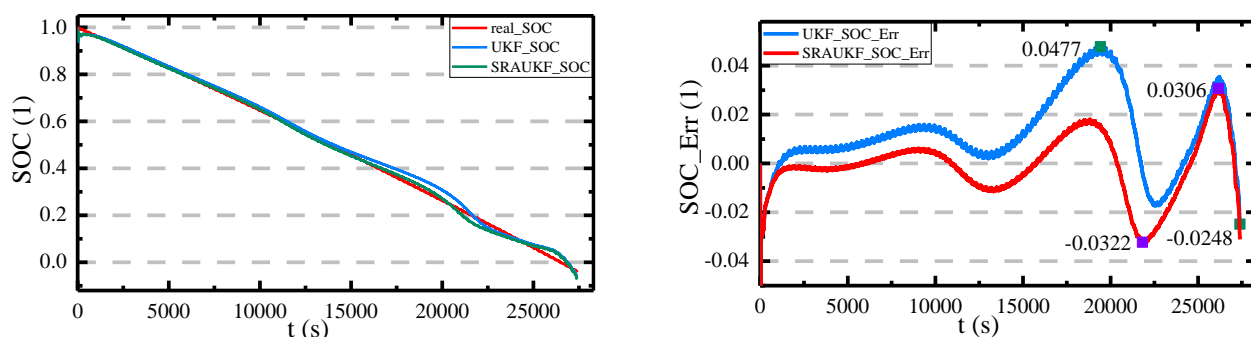
Figure 7. SOC estimation results under DST working condition

In Figure 7(a), red curve represents the real value, blue curve represents the estimated value based on the UKF algorithm, and green curve represents the estimated value based on the SR-AUKF algorithm.

In Figure 7 (b), blue curve represents the estimation error of the UKF algorithm, and red curve represents the estimation error of the SR-AUKF algorithm. It can be seen from Figure 7 that the overall estimation error of the SR-AUKF algorithm is lower than that of the UKF algorithm. Due to the internal chemical reaction of the battery, the estimated value of the battery SOC fluctuates greatly, and errors accumulate in the later period, so the SOC estimation error reaches the maximum value. However, the convergence effect of SR-AUKF is obviously better than that of the traditional UKF algorithm, and the error can be controlled within 5.65%, while the maximum error of UKF is as high as 7.44%. It verifies the value of the improved algorithm and has significance for the SOC estimation of lithium-ion batteries.

3.4. Algorithm validation under BBDST conditions

To further verify the stability and traceability of the SR-AUKF algorithm for SOC estimation under complex working conditions, the SOC estimation is implemented under the Beijing Bus Dynamic Stress Test (BBDST) working condition. The BBDST working condition was collected from the real data of the Beijing bus dynamic test, including the data under various operations such as starting, coasting, accelerating, and rapid acceleration, which is realistic and dynamic.



(a) Comparison between estimated and reference SOC

(b) SOC estimation error

Figure 8. SOC estimation results under DST working condition

It can be seen from Figure 8 that in the early stage of discharge, the two algorithms quickly track the real value, but the convergence speed of the SR-AUKF algorithm is significantly better than that of the traditional UKF. When the battery is at the end of discharge, the SOC estimation error fluctuates greatly. The main reason is that the nonlinearity of the battery is intense at the end of discharge. Many SOC estimation methods have low accuracy at the end of battery estimation. The accuracy of the algorithm in this paper can still be kept within 3.22% at the end of the estimation, and it can converge rapidly. In contrast, the average error and maximum error of the SR-AUKF algorithm are superior to those of the traditional UKF with faster tracking and better stability. There is a significant improvement.

4. CONCLUSION

Accurate estimation of the state of charge of high-power lithium-ion batteries is of great significance for the application and development of new energy vehicles. In this paper, the second-order RC equivalent model is used to characterize the dynamic characteristics of the battery, and the dynamic relationship of the internal parameters with time is obtained through RLS online parameter identification. To improve the SOC estimation accuracy, a joint estimation method of RLS and square root adaptive unscented Kalman is proposed. The algorithm makes full use of the residual information at multiple moments and configures corresponding weights for them according to the different amounts of information contained, and has good adaptive adjustment and correction functions. The experimental data under DST and BBDST are used for verification. The results show that the estimation error of the algorithm can be respectively controlled within 5.65% and 3.22%. Compared with the traditional algorithm, the estimation accuracy and stability are significantly improved. The research content of this paper has positive significance for the condition monitoring of lithium-ion batteries and the long-term development of new energy vehicles.

References

1. N. Li, Y. Zhang, F. He, L. Zhu, X. Zhang, Y. Ma and S. Wang, *Global Energy Interconnection*, 4 (2021) 619.
2. L. P. Chen, Y. Chen, A. M. Lopes, H. F. Kong and R. C. Wu, *Fractal and Fractional*, 5 (2021) 619.
3. M. Corno, N. Bhatt, S. M. Savaresi and M. Verhaegen, *Ieee Transactions on Control Systems Technology*, 23 (2015) 117.
4. Y. M. Fu, J. Xu, M. J. Shi and X. S. Mei, *Ieee Transactions on Industrial Electronics*, 69 (2022) 7019.
5. R. Havangi, *Electrical Engineering*, 104 (2022) 1001.
6. W. K. Ji, S. L. Wang, C. A. Y. Zou and H. T. Shi, *International Journal of Electrochemical Science*, 16 (2021) 210737.
7. D. P. Kong, S. H. Wang and P. Ping, *Journal of Energy Storage*, 44 (2021) 103389.
8. L. L. Li, Z. F. Liu and C. H. Wang, *Journal of Testing and Evaluation*, 48 (2020) 1712.
9. X. Y. Lin, Y. L. Tang, J. Ren and Y. M. Wei, *Journal of Energy Storage*, 41 (2021) 102840.
10. F. Liu, J. Ma, W. X. Su, H. N. Chen and M. W. He, *Energies*, 13 (2020) 1679.
11. A. Maheshwari, N. G. Paterakis, M. Santarelli and M. Gibescu, *Applied Energy*, 261 (2020) 114360.
12. Q. Ouyang, R. Ma, Z. X. Wu, G. T. Xu and Z. S. Wang, *Energies*, 13 (2020) 4968.
13. T. C. Ouyang, P. H. Xu, J. X. Chen, J. Lu and N. Chen, *Electrochimica Acta*, 353 (2020) 136576.
14. X. B. Peng, Y. W. Li, W. Yang and A. Garg, *Journal of Electrochemical Energy Conversion and Storage*, 18 (2021) 041007.
15. R. Sakile and U. K. Sinha, *Advanced Theory and Simulations*, 5 (2022) 2100397.
16. M. Wei, M. Ye, J. B. Li, Q. Wang and X. X. Xu, *Proceedings of the Institution of Mechanical Engineers Part D-Journal of Automobile Engineering*, 236 (2022) 241.
17. W. J. Zhang, L. Y. Wang, L. F. Wang, C. L. Liao and Y. W. Zhang, *Ieee Transactions on Industrial Electronics*, 69 (2022) 3677.
18. H. Zheng, X. Liu and M. Wei, *Chinese Physics B*, 24 (2015) 098801.
19. F. Zhu and J. Q. Fu, *Ieee Sensors Journal*, 21 (2021) 25449.
20. B. Jiang, H. F. Dai, X. Z. Wei and T. J. Xu, *Applied Energy*, 253 (2019) 113619.

21. H. Aung, K. S. Low and S. T. Goh, *Ieee Transactions on Power Electronics*, 30 (2015) 4774.
22. D. L. Liu, Y. C. Fan, S. L. Wang, L. L. Xia, J. S. Qiu and E. D. Bobobee, *International Journal of Electrochemical Science*, 16 (2021) 21097.
23. H. W. He, H. Z. Qin, X. K. Sun and Y. P. Shui, *Energies*, 6 (2013) 5088.
24. S. L. Liu, N. X. Cui and C. H. Zhang, *Energies*, 10 (2017) 1345

© 2022 The Authors. Published by ESG (www.electrochemsci.org). This article is an open access article distributed under the terms and conditions of the Creative Commons Attribution license (<http://creativecommons.org/licenses/by/4.0/>).